AIAA 93-0912
Three-Dimensional Solidification With Magnetic Fields and Reduced Gravity

G. Dulikravich and V. Ahuja
The Pennsylvania State University
University Park, PA
and
S. Lee
Defense Research Agency
Taejon, Korea

31st Aerospace Sciences Meeting & Exhibit
January 11-14, 1993 / Reno, NV

THREE-DIMENSIONAL SOLIDIFICATION WITH MAGNETIC FIELDS AND REDUCED GRAVITY

George S. Dulikravich[1], Vineet Ahuja[2] and Seungsoo Lee[3]

Department of Aerospace Engineering
The Pennsylvania State University, University Park, PA 16802, USA

Abstract

Two interacting systems of partial differential equations governing three-dimensional laminar flow of an incompressible viscous fluid undergoing solidification or melting under the influence of externally applied magnetic fields have been formulated analytically and integrated numerically. The model allows for separate temperature-dependent physical properties within the melt and the solid phase. It includes effects of Joule heating, latent heat release, microgravity and magnetic ponderomotive force. The amount of latent heat released is an arbitrary function of temperature. Mushy region is automatically captured by varying viscosity several orders of magnitude in the mushy region. It was found numerically that the presence of an external steady magnetic field: a) diminishes flow field vorticity, b) causes higher velocity gradients within the mushy region, c) influences the amount of accrued solid phase, and d) influences the solid/liquid interface shape. These numerical results demonstrate possibilities for a practical automatic control of phase change processes using a combination of magnetic and gravitational fields.

Nomenclature

c = specific heat, J kg^{-1} K^{-1}
Ec = Eckert number
Fr = Froude number
$\mathbf{g}$ = gravity force per unit volume, m s^{-2}
Gr = Grashof number
$\mathbf{H}$ = magnetic field, H kg^{-1}
H_t = Hartmann number
k = heat conductivity coefficient, W m^{-1} K^{-1}
l = length, m
L = latent heat of liquid/solid phase change, J kg^{-1}
p = pressure, kg m^{-1} s^{-2}
P_m = magnetic Prandtl number
Pr = Prandtl number
R = volume fraction of the liquid phase
Ra = Gr Pr = Rayleigh number
Re = hydrodynamic Reynolds number
S_{te} = Stefan number
t = time, s
T = absolute temperature, K
ΔT = $T_s - T_l$ = temperature difference, K
$\mathbf{v}$ = (u,v,w) = velocity vector, m s^{-1}
V = volume, m^3
x,y,z = Cartesian coordinates, m
α = thermal expansion coefficient, K^{-1}
β = artificial compressibility parameter
η = viscosity coefficient, kg m^{-1} s^{-1}
ξ, η, ζ = non-orthogonal grid coordinates
μ = magnetic permeability coefficient, H m^{-1}
ρ = density, kg m^{-3}
σ = electrical conductivity, Ω^{-1} m^{-1}
θ = non-dimensional temperature
ϕ = gravity potential ($g_i = \phi_{,i}$)

subscripts
o = reference values
c = cold wall
h = hot wall
i = component of a vector
j = component of a vector
l = liquidus
s = solidus

superscripts
* = nondimensional values
' = function of nondimensional temperature
= transpose of a matrix or a vector

Introduction

The objective of this paper is to elaborate on a mathematical model and an accompanying numerical algorithm capable of simulating fully three-dimensional melt flow control during melting and solidification via an arbitrarily distributed and oriented externally applied magnetic field. It has been well known analytically [1,2] and demonstrated computationally [3-11] that the magnetic field can eliminate vorticity from the flow field and reduce the magnitude of the fluid motion so that the solid/liquid front shape and its propagation speed could be manipulated. The formulation presented in this paper extrapolates on our previous work [7-11] which was based on the fundamental concepts of MagnetoHydroDynamics (MHD) as formulated by Stuetzer [2] and an extended Boussinesq approximation formulation [12] that allows for temperature-dependent physical properties. Our formulation simultaneously predicts detailed velocity, pressure, temperature and magnetic fields for the moving melt, while capturing the forming solid phase by using a single computer code. The same mathematical formulation and computer code can simulate the reverse process of melting of the solid phase. In this work we have formulated the entire

[1] Associate Professor. Associate Fellow AIAA.

[2] Graduate Assistant. Student member AIAA.

[3] Postdoctoral Fellow. Presently with Aerodynamics Department, Agency for Defense Development, Taejon, Republic of Korea.

problem as three-dimensional and time-dependent although our computational results will be for steady situations only.

Analytical Model

Starting with the Maxwell's equations and the Ohm's law, the magnetic field transport equation can be derived [1,2,7] as

$$H_{i,t} - (v_j H_i - v_i H_j)_{,j} = \frac{1}{\mu\sigma} H_{i,jj}. \qquad (1)$$

where subscripts after the comma designate partial differentiation with respect to the variable or variables that follow the comma. The fluid flow partial differential equations (Navier-Stokes) and the magnetic field transport partial differential equations (Maxwell) can be non-dimensionalized. If the flow has a mean stream, the non-dimensionalization will lead to the introduction of the hydrodynamic Reynolds number because of the well defined reference velocity. Thus,

$$v_i^* = \frac{v_i}{v_o} \qquad x_i^* = \frac{x_i}{l_o} \qquad t^* = \frac{t\, v_o}{l_o} \qquad (2)$$

$$p^* = \frac{p}{\rho_o v_o^2} \qquad g^* = \frac{g_i}{g_o} \qquad H_i^* = \frac{H_i}{H_o} \qquad (3)$$

$$\theta = \frac{T - T_o}{\Delta T} \qquad \sigma^* = \frac{\sigma}{\sigma_o} \qquad \mu^* = \frac{\mu}{\mu_o} \qquad (4)$$

Here, we chose $\Delta T = T_s - T_l$ and $T_o = T_s$. In this work only incompressible flow will be considered while accounting for thermal buoyancy via an extended Boussinesq approximation in the form which is valid even when melt and solid properties vary as arbitrary functions of non-dimensional temperature [12]. Thus,

$$\rho = \rho_o \rho'(\theta) \qquad c = c_o c'(\theta) \qquad \eta = \eta_o \eta'(\theta) \qquad (5)$$

$$k = k_o k'(\theta) \qquad \sigma = \sigma_o \qquad \mu = \mu_o \qquad (6)$$

Here we have assumed only σ and μ not to vary with the temperature. A function describing variation of density as a function of non-dimensional temperature is then

$$\rho' = 1 + \left.\frac{\partial(\rho/\rho_o)}{\partial\theta}\right|_o \theta_s + \left.\frac{\partial(\rho/\rho_o)}{\partial\theta}\right|_s (\theta - \theta_s)$$

$$= 1 - \alpha_o^* \theta_s - \alpha_s^* (\theta - \theta_s) = 1 - (\alpha_o^* - \alpha_s^*)\theta_s - \alpha_s^* \theta \qquad (7)$$

with a similar expression for k'. The latent heat released or absorbed per unit mass of mushy region (where $T_l > T > T_s$) is proportional to the local volumetric liquid/solid ratio often modeled [13] as

$$R = \frac{V_l}{V_l + V_s} = \left(\frac{\theta - \theta_s}{\theta_l - \theta_s}\right)^n \qquad (8)$$

where the exponent n is typically $0.2 < n < 5$. With the following non-dimensional groups

$$Re = \frac{\rho_o v_o l_o}{\eta_o} \qquad Fr^2 = \frac{v_o^2}{g\, l_o} \qquad Ec = \frac{v_o^2}{c_o \Delta T} \qquad (9)$$

$$Pr = \frac{\eta_o c_o}{k_o} \qquad Ste = \frac{c_o \Delta T}{L} \qquad P_m = \frac{\mu_o \sigma_o \eta_o}{\rho_o} \qquad (10)$$

$$Gr = \frac{\rho_o^2 \alpha\, g_o\, \Delta T\, l_o^3}{\eta_o^2} \qquad H_t = \mu_o l_o H_o \left(\frac{\sigma_o}{\eta_o}\right)^{1/2} \qquad (11)$$

after introducing $\frac{Gr\theta}{Re^2}$ instead of $\frac{\alpha_s^* \theta}{Fr^2}$ in the thermal buoyancy term, assuming that $\alpha_s^* \theta << 1$, and dropping the asterisk symbol, the non-dimensional Navier-Stokes equations for phase-changing MHD flows become

$$v_{i,i} = 0 \qquad (12)$$

$$v_{i,t} + (v_i v_j)_{,j} = \frac{1}{Re}(\eta' v_{i,j})_{,j} - \bar{\bar{p}}_{,i} + \frac{R\, Gr\, \theta}{Re^2} g_i + \frac{H_t^2}{P_m\, Re^2} (H_i H_k)_{,k} \qquad (13)$$

$$\theta_{,t} + v_i \theta_{,i} = \frac{R}{Re\, Pr\, c_e'} (k_l' \theta_{,i})_{,i} + \frac{(1-R)}{Re\, Pr\, c_e'} (k_s' \theta_{,i})_{,i} + R \frac{Re\, \eta'}{Ec\, c_e'} (v_{i,j} + v_{j,i}) v_{i,j} + \frac{1}{c_e'} \frac{H_t^2\, Ec}{P_m^2\, Re^3} e_{ijk} e_{ilm} H_{k,j} H_{m,l} \qquad (14)$$

Non-dimensional hydrostatic, hydrodynamic, and magnetic pressures can be combined to give

$$\bar{\bar{p}} = p + \frac{\phi}{Fr^2} + \frac{H_t^2}{P_m\, Re^2} H_i H_i \qquad (15)$$

where ϕ is the non-dimensional gravity potential defined as $g_i = \phi_{,i}$. If S=1 for a melting cell and S=0 for a solidifying cell, the enthalpy method [14] leads to the introduction of a non-dimensional equivalent specific heat, $c_e' = c_e / c_o$, which can be defined as

$$c_e' = \left(R\, c_l' - \rho_l' \frac{S}{Ste} \frac{\partial R}{\partial\theta}\right) + \left((1-R)\, c_s' + \rho_s' \frac{(1-S)}{Ste} \frac{\partial R}{\partial\theta}\right) \qquad (16)$$

The magnetic field transport equations in their non-dimensional form become

$$H_{,t} - (v_j H_i - v_i H_j)_{,j} = \frac{1}{P_m\, R_e} H_{i,jj} \qquad (17)$$

Viscosity in the mushy region was modeled according to an exponential law, that is, $\eta/\eta_l = 10 \exp(R)$.

Numerical Model

Equations (12), (13), (14) and (17) represent a system of eight coupled non-linear partial differential equations [7]. This global system has been split into two systems in order to simplify computer programming. The first system represents the non-dimensional Navier-Stokes equations for incompressible flows with thermal buoyancy, magnetic field effects and possible solidification or melting. It can be written in a fully conservative form in terms of the non-orthogonal grid-following boundary-fitted coordinate system as

$$\frac{\partial \tilde{\mathbf{Q}}}{\partial t} + \frac{\partial \tilde{\mathbf{E}}}{\partial \xi} + \frac{\partial \tilde{\mathbf{F}}}{\partial \eta} + \frac{\partial \tilde{\mathbf{G}}}{\partial \zeta} = \tilde{D}_{NS} + \tilde{S}_{NS} \tag{18}$$

where $\xi = \xi(x,y,z)$, $\eta = \eta(x,y,z)$, $\zeta = \zeta(x,y,z)$, $\tilde{\mathbf{Q}}$ is the transformed solution vector, $\tilde{\mathbf{E}}$, $\tilde{\mathbf{F}}$ and $\tilde{\mathbf{G}}$ are the transformed flux vectors, and $\tilde{\mathbf{S}}$ is the transformed source vector. The diffusion vector in general curvilinear coordinates is defined as

$$\tilde{D}_{NS} = \tilde{\bar{\bar{D}}}_{NS}\left[\frac{\tilde{D}_{NS}}{J} g_{ij} \left(J\tilde{Q}\right)_{,j}\right]_{,i} \tag{19}$$

where $J = \det\left[\left(\frac{\partial(\xi,\eta,\zeta)}{\partial(x,y,z)}\right)\right]$ is the determinant of the Jacobian geometric transformation matrix and the metric tensor components are defined as

$$g_{ij} = \frac{\partial \bar{x}_i}{\partial \hat{x}_j}\frac{\partial \bar{x}_j}{\partial \hat{x}_i} \tag{20}$$

Here, $\bar{x}_i = \bar{x}_i(x, y, z)$ is the Cartesian coordinate vector and $\hat{x}_i = \hat{x}_i(\xi, \eta, \zeta)$ is the curvilinear coordinate vector. The contravariant components U, V, W and $\hat{H}_\xi$, $\hat{H}_\eta$, $\hat{H}_\zeta$ are defined as

$$\begin{Bmatrix} U \\ V \\ W \end{Bmatrix} = \begin{bmatrix} \xi,x & \xi,y & \xi,z \\ \eta,x & \eta,y & \eta,z \\ \zeta,x & \zeta,y & \zeta,z \end{bmatrix} \begin{Bmatrix} u \\ v \\ w \end{Bmatrix} \tag{21}$$

$$\begin{Bmatrix} \hat{H}_\xi \\ \hat{H}_\eta \\ \hat{H}_\zeta \end{Bmatrix} = \begin{bmatrix} \xi,x & \xi,y & \xi,z \\ \eta,x & \eta,y & \eta,z \\ \zeta,x & \zeta,y & \zeta,z \end{bmatrix} \begin{Bmatrix} H_x \\ H_y \\ H_z \end{Bmatrix} \tag{22}$$

For the Navier-Stokes equations, the vectors are defined as follows

$$\tilde{\mathbf{Q}} = \frac{1}{J}\begin{Bmatrix} 0 \\ u \\ v \\ w \\ \theta \end{Bmatrix} \quad \tilde{\mathbf{E}} = \frac{1}{J}\begin{Bmatrix} U \\ Uu+\xi,_x \bar{\bar{p}} \\ Uv+\xi,_y \bar{\bar{p}} \\ Uw+\xi,_z \bar{\bar{p}} \\ U\theta \end{Bmatrix} \quad \tilde{\mathbf{F}} = \frac{1}{J}\begin{Bmatrix} V \\ Vu+\eta,_x \bar{\bar{p}} \\ Vv+\eta,_y \bar{\bar{p}} \\ Vw+\eta,_z \bar{\bar{p}} \\ V\theta \end{Bmatrix} \tag{23}$$

$$\tilde{\mathbf{G}} = \frac{1}{J}\begin{Bmatrix} W \\ Wu+\zeta,_x \bar{\bar{p}} \\ Wv+\zeta,_y \bar{\bar{p}} \\ Ww+\zeta,_z \bar{\bar{p}} \\ W\theta \end{Bmatrix} \tag{24}$$

$$\tilde{\bar{\bar{D}}}_{NS} = \mathrm{diag}\left[0 \ \frac{R}{Re} \ \frac{R}{Re} \ \frac{R}{Re} \ \left\{\frac{R}{RePr\, c_e'} \quad \frac{(1-R)}{RePr\, c_e'}\right\}^{\#}\right] \tag{25}$$

$$\tilde{D}_{NS} = \mathrm{diag}\left[0 \ \eta' \ \eta' \ \eta' \ \begin{Bmatrix} k_l' \\ k_s' \end{Bmatrix}\right] \tag{26}$$

The system of equations (18) based on the above value of $\tilde{\mathbf{Q}}$ is singular since there is no time derivative term in the mass conservation equation and the system cannot be integrated simultaneously. Consequently, an artificial compressibility [15] term, $\frac{\partial}{\partial t}\left(\frac{\bar{\bar{p}}}{\beta J}\right)$, is added to the mass conservation so that the first term of the vector $\tilde{\mathbf{Q}}$ becomes $\tilde{Q}_1 = \bar{\bar{p}}/(\beta J)$. Here, β is a user specified parameter that depends on the problem geometry, grid, flow parameters, etc. [16]. In the steady state limit, the time variation of $\tilde{Q}_1$ term tends to zero and does not influence the accuracy of the steady state solution. The non-zero components of the source vector $\tilde{S}_{NS}$ are

$$\tilde{S}_{NS2} = \frac{H_t^2}{P_m\, Re^2}\left(\frac{\partial}{\partial\xi}\left(\frac{\hat{H}_\xi\, H_x}{J}\right) + \frac{\partial}{\partial\eta}\left(\frac{\hat{H}_\eta\, H_x}{J}\right) + \frac{\partial}{\partial\zeta}\left(\frac{\hat{H}_\zeta\, H_x}{J}\right)\right) - \frac{R\, Gr\, \theta}{J\, Re^2} g_x \tag{27}$$

$$\tilde{S}_{NS3} = \frac{H_t^2}{P_m\, Re^2}\left(\frac{\partial}{\partial\xi}\left(\frac{\hat{H}_\xi\, H_y}{J}\right) + \frac{\partial}{\partial\eta}\left(\frac{\hat{H}_\eta\, H_y}{J}\right) + \frac{\partial}{\partial\zeta}\left(\frac{\hat{H}_\zeta\, H_y}{J}\right)\right) - \frac{R\, Gr\, \theta}{J\, Re^2} g_y \tag{28}$$

$$\tilde{S}_{NS4} = \frac{H_t^2}{P_m\, Re^2}\left(\frac{\partial}{\partial\xi}\left(\frac{\hat{H}_\xi\, H_z}{J}\right) + \frac{\partial}{\partial\eta}\left(\frac{\hat{H}_\eta\, H_z}{J}\right) + \frac{\partial}{\partial\zeta}\left(\frac{\hat{H}_\zeta\, H_z}{J}\right)\right) - \frac{R\, Gr\, \theta}{J\, Re^2}\, g_z \qquad (29)$$

$$\tilde{S}_{NS5} = \frac{J}{c_e'}\frac{H_t^2\, Ec}{P_m^2\, Re^3}\left(\tilde{P}_1^2 + \tilde{P}_2^2 + \tilde{P}_3^2\right) \qquad (30)$$

Here, g_x, g_y, g_z are the Cartesian components of the non-dimensional gravity vector, while

$$\tilde{P}_1 = \frac{\partial}{\partial\xi}\left(\frac{H_z\xi_{,y} - H_y\xi_{,z}}{J}\right) + \frac{\partial}{\partial\eta}\left(\frac{H_z\eta_{,y} - H_y\eta_{,z}}{J}\right) + \frac{\partial}{\partial\zeta}\left(\frac{H_z\zeta_{,y} - H_y\zeta_{,z}}{J}\right) \qquad (31)$$

$$\tilde{P}_2 = \frac{\partial}{\partial\xi}\left(\frac{H_x\xi_{,z} - H_z\xi_{,x}}{J}\right) + \frac{\partial}{\partial\eta}\left(\frac{H_x\eta_{,z} - H_z\eta_{,x}}{J}\right) + \frac{\partial}{\partial\zeta}\left(\frac{H_x\zeta_{,z} - H_z\zeta_{,x}}{J}\right) \qquad (32)$$

$$\tilde{P}_3 = \frac{\partial}{\partial\xi}\left(\frac{H_y\xi_{,x} - H_x\xi_{,y}}{J}\right) + \frac{\partial}{\partial\eta}\left(\frac{H_y\eta_{,x} - H_x\eta_{,y}}{J}\right) + \frac{\partial}{\partial\zeta}\left(\frac{H_y\zeta_{,x} - H_x\zeta_{,y}}{J}\right) \qquad (33)$$

Similarly, the transformed system of magnetic field transport equations can be expressed as

$$\frac{\partial\tilde{Q}}{\partial t} + \frac{\partial\tilde{E}}{\partial\xi} + \frac{\partial\tilde{F}}{\partial\eta} + \frac{\partial\tilde{G}}{\partial\zeta} = \tilde{\tilde{D}}_{MAG} + \tilde{S}_{MAG} \qquad (34)$$

where the solution vector $\tilde{Q}$, the flux vectors $\tilde{E}$, $\tilde{F}$, $\tilde{G}$, and matrices $\tilde{\tilde{D}}_{MAG}$ and $\tilde{D}_{MAG}$ are defined as

$$\tilde{Q} = \frac{1}{J}\begin{Bmatrix} H_x \\ H_y \\ H_z \end{Bmatrix} \quad \tilde{E} = \frac{1}{J}\begin{Bmatrix} H_xU - u\hat{H}_\xi \\ H_yU - v\hat{H}_\xi \\ H_zU - w\hat{H}_\xi \end{Bmatrix} \quad \tilde{F} = \frac{1}{J}\begin{Bmatrix} H_xV - u\hat{H}_\eta \\ H_yV - v\hat{H}_\eta \\ H_zV - w\hat{H}_\eta \end{Bmatrix} \qquad (35)$$

$$\tilde{G} = \frac{1}{J}\begin{Bmatrix} H_xW - u\hat{H}_\zeta \\ H_yW - v\hat{H}_\zeta \\ H_zW - w\hat{H}_\zeta \end{Bmatrix} \quad \tilde{\tilde{D}}_{MAG} = I \quad \tilde{D}_{MAG} = \frac{1}{P_m\, Re} I \qquad (36)$$

while $\tilde{S}_{MAG} = 0$. In the case of flows where there is no identifiable reference velocity (as in the case of a thermally induced flow inside a closed container) and rather than guessing the value of the Reynolds number it is often advantageous to avoid it by performing the non-dimensionalization with respect to different reference variables. Specifically, if the characteristic velocity is chosen as the ratio of thermal diffusivity and the characteristic length, that is, if $v_o = k_o/(\rho_o\, c_o\, l_o)$, the coefficient matrix $\tilde{\tilde{D}}_{NS}$ becomes

$$\tilde{\tilde{D}}_{NS} = diag\left[0\ RP_r\ RP_r\ RP_r\ \left\{\frac{R}{c_e'}\ \frac{(1-R)}{c_e'}\right\}^{\#}\right] \qquad (37)$$

while $\tilde{D}_{NS}$, $\tilde{\tilde{D}}_{MAG}$, $\tilde{D}_{MAG}$ and $\tilde{S}_{MAG}$ remain unchanged. Also, terms of the transformed source vector $\tilde{S}_{NS}$ in the Navier-Stokes equations remain the same as in equations (27-30) except that Ra Pr should now be used instead of Gr/Re^2. Here, the Rayleigh number is defined as Ra = Gr Pr.

In the case of a three-dimensional problem, eight partial differential equations need to be satisfied simultaneously. This was accomplished by integrating a system of five fluid flow equations (Eq. 18) and a system of three magnetic field equations (Eq. 34) in an alternating fashion [7] and after each iteration transferring the information through source-like terms $\tilde{S}_{NS}$. By adding the artificially time-dependent term in the mass conservation, the entire Navier-Stokes system becomes non-singular and of a hyperbolic type so that it can be integrated in time using an artificial time marching [7] technique based on an explicit four-stage Runge-Kutta time-stepping algorithm [17]. The explicit time integration scheme was used because it can be efficiently vectorized and easily modified when additional equations need to be incorporated in a system. A small amount of fourth order artificial dissipation [17] was added to the Navier-Stokes system at higher Reynolds number flows to suppress numerical oscillations that appears due to even-odd decoupling caused by central space differencing.

Boundary Conditions

Solid walls: Along the solid walls, the velocity components were set to zero. The pressure gradient normal to the walls calculated from the momentum equations were used to compute pressure at the solid boundaries. This gives physically correct wall pressure distribution rather than assuming zero pressure gradient normal to the wall. Depending on which type of thermal boundary condition was imposed at the wall, the wall temperature was either specified or obtained from the specified surface heat flux and the points on the first grid line off the boundary.

Inlet and exit boundaries: In the case of a melt flow through a three-dimensional passage with an open inlet and an exit, both characteristic and non-reflective boundary conditions have been implemented at the exit.

Characteristic boundary conditions [7] can be determined by rewriting the system (18) in a nonconservative (characteristic) form as

$$\frac{\partial\tilde{Q}}{\partial t} + \tilde{A}\frac{\partial\tilde{Q}}{\partial\xi} + \tilde{B}\frac{\partial\tilde{Q}}{\partial\eta} + \tilde{C}\frac{\partial\tilde{Q}}{\partial\zeta} = \tilde{D}_{NS} + \tilde{S} \qquad (38)$$

The eigenmatrix $\tilde{\Lambda}$ corresponding to the flux vector Jacobian coefficient matrix $\tilde{A}$ is

$$\tilde{\Lambda} = \text{diag}\,[U-a,\ U+a,\ U,\ U,\ U] \tag{39}$$

where a is the equivalent local speed of sound

$$a = (U^2 + \beta\,(\xi_{,x}^2 + \xi_{,y}^2 + \xi_{,z}^2))^{1/2} \tag{40}$$

From the eigenvalues it is obvious that there are four incoming characteristics corresponding to four positive eigenvalues. Thus, four variables (u,v,w,θ) have to be specified at the inlet assuming that ξ is in the direction of the mean flow there. Nevertheless, the first eigenvalue is negative at the inlet meaning that one variable ($\bar{\bar{p}}$) has to be computed at the inlet from a characteristic form of the equations. Similarly, at the exit boundary, the combined pressure ($\bar{\bar{p}}$) should be specified while the velocity components and the temperature should be obtained by integrating the characteristic equations.

The similarity transformation matrix $\mathbf{M}_{\xi}^{-1}$ that converts the ξ-direction generalized flux vector $\tilde{\mathbf{E}}$, into its characteristic non-conservative form is given by

$$\mathbf{M}_{\xi}^{-1} = \begin{bmatrix} m_{11} & m_{12} & m_{13} & m_{14} & m_{15} \\ m_{21} & m_{22} & m_{23} & m_{24} & m_{25} \\ m_{31} & m_{32} & m_{33} & m_{34} & m_{35} \\ m_{41} & m_{42} & m_{43} & m_{44} & m_{45} \\ m_{51} & m_{52} & m_{53} & m_{54} & m_{55} \end{bmatrix} \tag{41}$$

where the coefficients are

$$m_{11} = -U - a \qquad m_{12} = \xi_{,x} \qquad m_{13} = \xi_{,y}$$

$$m_{14} = \xi_{,z} \qquad m_{15} = 0$$

$$m_{21} = -U + a \qquad m_{22} = \xi_{,x} \qquad m_{23} = \xi_{,y}$$

$$m_{24} = \xi_{,z} \qquad m_{25} = 0$$

$$m_{31} = \beta\,((\xi_{,y}\,k_{23} - \xi_{,z}\,k_{12})\,u + (\xi_{,z}\,k_{31} - \xi_{,x}\,k_{23})\,v + (\xi_{,x}\,k_{12} - \xi_{,y}\,k_{31})\,w)$$

$$m_{32} = U\,(k_{12}w - k_{23}v) - \beta\,(\xi_{,y}\,k_{23} - \xi_{,z}\,k_{12})$$
$$m_{33} = U\,(k_{23}u - k_{31}w) - \beta\,(\xi_{,z}\,k_{31} - \xi_{,x}\,k_{23})$$
$$m_{34} = U\,(k_{31}v - k_{12}u) - \beta\,(\xi_{,x}\,k_{12} - \xi_{,y}\,k_{31})$$
$$m_{35} = 0$$

$$m_{41} = \beta\,((\xi_{,z}\,k_{23} - \xi_{,y}\,k_{31})\,u + (\xi_{,x}\,k_{31} - \xi_{,z}\,k_{12})\,v + (\xi_{,y}\,k_{12} - \xi_{,x}\,k_{23})\,w)$$

$$m_{42} = U\,(k_{31}\,v - k_{23}\,w) - \beta\,(\xi_{,z}\,k_{23} - \xi_{,y}\,k_{31})$$

$$m_{43} = U\,(k_{12}\,w - k_{31}\,u) - \beta\,(\xi_{,x}\,k_{31} - \xi_{,z}\,k_{12})$$

$$m_{44} = U\,(k_{23}\,u - k_{12}\,v) - \beta\,(\xi_{,y}\,k_{12} - \xi_{,x}\,k_{23})$$

$$m_{45} = 0$$

$$m_{51} = (U^2 - a^2)\theta \qquad m_{52} = -\xi_{,x}\,U\theta \qquad m_{53} = -\xi_{,y}\,U\theta$$

$$m_{54} = -\xi_{,z}\,U\theta \qquad m_{55} = a^2 \tag{42}$$

where

$$k_{12} = \xi_{,z}^2 - \xi_{,x}\xi_{,y}$$
$$k_{23} = \xi_{,x}^2 - \xi_{,y}\xi_{,z}$$
$$k_{31} = \xi_{,y}^2 - \xi_{,z}\xi_{,x} \tag{43}$$

If equations (18) are premultiplied by the similarity transformation matrix $\mathbf{M}_{\xi}^{-1}$, the characteristic form of the equations is obtained. The equation corresponding to the negative eigenvalue is to be selected at the inlet, while at the exit the equations corresponding to the positive eigenvalues are chosen. The selection procedure can be conducted using the selection matrix **L**. If the boundary condition vector is Ω, then

$$\Omega^{t+1} = \Omega^t + \frac{\partial \Omega}{\partial \tilde{Q}}\,\Delta\tilde{Q} \tag{44}$$

or

$$\frac{\partial \Omega}{\partial \tilde{Q}}\,\Delta\tilde{Q} = -\,\Omega^t \tag{45}$$

Equations (44) are added to the system of transformed equations, so that,

$$\left[\mathbf{L}\mathbf{M}_{\xi}^{-1}\frac{\partial \Omega}{\partial \tilde{Q}}\right]\Delta\tilde{Q} = -\alpha_k \Delta t\left[\mathbf{M}_{\xi}^{-1}\mathbf{R}^{k-1} + \frac{\Omega^t}{\alpha_k \Delta t}\right] \tag{46}$$

Here, t is the iteration level, α_k are the coefficients in the Runge-Kutta k-stage time-stepping scheme, and **R** is the residual vector of system (18). At the inlet plane,

$$\mathbf{L} = \text{diag}[1,0,0,0,0] \tag{47}$$

$$\Omega = [\ 0,\ u-u_p,\ v-v_p,\ w-w_p,\ \theta-\theta_p\ ]^{\#} \tag{48}$$

At the exit plane

$$\mathbf{L} = \text{diag}[0,\ 1,\ 1,\ 1,\ 1] \tag{49}$$

$$\Omega = [\ \bar{\bar{p}} - \bar{\bar{p}}_p,\ 0,\ 0,\ 0,\ 0\ ]^{\#} \tag{50}$$

so that

$$\frac{\partial \Omega}{\partial \tilde{Q}} = \text{diag}[\beta J, 0, 0, 0, 0]. \qquad (51)$$

Nevertheless, the characteristic boundary conditions at the exit plane require specification of the melt pressure on the entire exit plane, which cannot be performed correctly since the correct pressure distribution there is unknown *a priori* especially if the flow at the exit is not fully developed. A remedy is to use a different type of exit boundary conditions.

The non-reflecting boundary conditions do not force us to specify any of the physical variables at the exit plane. Instead, an additional equation needs to be solved there. The non-reflecting boundary condition demands that the amplitude of an incoming wave be constant in time. This condition allows computation to handle the variable pressure at the exit boundary. The outgoing waves depend only on information at the boundary and within the domain. Thus, those equations which represent outgoing waves can be solved at the exit boundary as they are to give three velocity components and temperature at the exit. At the inlet boundary, a characteristic boundary treatment was employed whereby three velocity components and one temperature are specified and pressure is obtained by solving the characteristic form of the equation which has a negative eigenvalue.

For one-dimensional problems, wave propagation direction is well defined. For multidimensional problems there is no unique direction of propagation because the coefficient matrices $\tilde{A}, \tilde{B}, \tilde{C}$ cannot be simultaneously diagonalized. Boundary condition analysis requires that any one coordinate direction be diagonalizable at a time. Eigenvectors corresponding to the Jacobian coefficient matrix $\tilde{A}$ are solutions of $\left[\tilde{A} - \tilde{\lambda} I\right]\{X\} = 0$. Premultiplying the governing equation (18) with the inverse of a similarity matrix $\tilde{S}$ of $\tilde{A}$ gives

$$\tilde{S}^{-1}\frac{\partial \tilde{Q}}{\partial t} + \tilde{S}^{-1}\tilde{A}\,\tilde{S}\,\tilde{S}^{-1}\frac{\partial \tilde{Q}}{\partial \xi} + \tilde{S}^{-1}\tilde{H} = 0 \qquad (52)$$

where

$$\tilde{H} = \tilde{B}\frac{\partial \tilde{Q}}{\partial \eta} + \tilde{C}\frac{\partial \tilde{Q}}{\partial \zeta} - \tilde{D}_{NS} - \tilde{S} \qquad (53)$$

Then we can define a column vector L as follows

$$L = = \tilde{S}^{-1}\tilde{A}\,\tilde{S}\,\tilde{S}^{-1}\frac{\partial \tilde{Q}}{\partial \xi} \qquad (54)$$

Components of L defined as above are used for the equations corresponding to the outgoing waves while for the equations corresponding to incoming waves the characteristic boundary treatment and non-reflecting boundary treatment have different approaches. In characteristic boundary treatment for incoming waves, flow properties are specified instead of solving the equations. On the other hand, the non-reflecting boundary treatment defines L's differently for only these equations corresponding to incoming waves [18,19]

$$L_i = -\left(\tilde{S}^{-1}\tilde{H}\right)_i \qquad (55)$$

Here the subscript i represents the equation corresponding to the incoming wave. This condition constrains the amplitude of the incoming wave to remain constant with time so that the outgoing waves are not allowed to reflect back into the domain. This formulation of non-reflecting exit boundary condition was used in the present work allowing for the non-uniform pressure on the exit plane.

The system of the magnetic field equations (34) is also hyperbolic in time. The eigenvalues of the Jacobian matrix of this system are $\tilde{\Lambda} = \text{diag}[U, U, 0]$ in the case of ξ–direction. At the inlet plane, therefore, two components of the magnetic field vector should be specified, while the axial component H_x of the magnetic field vector has to be evaluated from the characteristic equation. The transformation matrix for the magnetic transport equations is given by

$$M_{\xi}^{-1} = \begin{bmatrix} k_{23}v - k_{12}w & k_{31}w - k_{23}u & k_{12}u - k_{31}v \\ k_{23}w - k_{31}v & k_{31}u - k_{12}w & k_{12}v - k_{23}u \\ -\xi_{,x}\,k_{123} & -\xi_{,y}\,k_{123} & -\xi_{,z}\,k_{123} \end{bmatrix} \qquad (56)$$

where k_{12}, k_{23}, k_{31} are defined like in the equation (43) and

$$k_{123} = k_{12} + k_{23} + k_{31} \qquad (57)$$

Here

$$L = \text{diag}[1, 1, 0] \qquad (58)$$

$$\Omega = \{ H_x - H_{xp},\ H_y - H_{yp},\ 0 \}^{\#} \qquad (59)$$

At the exit plane, all three magnetic field components are updated by integrating the governing equations. When the wall is a perfect conductor, the tangential component of the magnetic field is discontinuous while the normal component is continuous. If $\langle\,\rangle$ denotes the jump across the boundary, then at the wall boundary

$$\mathbf{n} \times \langle \mathbf{E} \rangle = 0 \qquad \mathbf{n} \cdot \mathbf{H} = 0 \qquad (60)$$

If the wall is a perfect insulator, then the magnetic field has no discontinuities at the boundary, that is $\langle \mathbf{H} \rangle = 0$.

Numerical Results

Based on the elaborated analytical model and the numerical algorithm a fully three-dimensional MHD flow analysis computer code has been developed [7].

Numerical results from this code were compared with known analytical solutions and proved to be highly accurate [7]. This code was then augmented to incorporate thermally induced buoyancy, temperature-dependent physical properties of the melt and the solid phase and the effects of latent heat release with an adequate account of the mushy region.

Two basic configurations were studied with this code: a cubical closed container (Fig. 1a) with sides of length l = 0.01 m and a straight duct having square cross section (Fig.1b) with dimensions 0.01 m x 0.01 m x 0.0475 m. The cubical closed container was completely filled with the melt and the duct was assumed to be horizontal with the melt flowing from left to right in the positive x-direction. Gravity was assumed to act vertically downward in the positive z-direction. If not indicated otherwise, the solid walls were thermally insulated. All runs were performed with CFL number 2.8, von Neuman number 0.4, artificial compressibility parameter $\beta = 5$ and with the coefficient of fourth order artificial [17] dissipation $\nu = 0.0001$. The values of the reference parameters were: $v_o = 0.01$ ms^{-1}, $l_o = 0.01$ m, $g_o = 9.81$ m s^{-2} and the exponent used in the model for latent heat release (Eq. 8) was $n = 5$. Values of the non-dimensional parameters used in the test cases are summarized in Table 1. Physical properties used in the case of a molten steel are summarized in Table 2.

Closed container without solidification: As a basic test of the capability of the computer code to predict three dimensional buoyancy driven flows without any phase change in a cubical closed container we used the test case of Ozoe and Okada [3]. Two numerical tests were carried out in the cubical enclosure with one of the vertical walls ($x^* = 0$) uniformly heated ($\theta = 0.5$) and the opposite vertical wall uniformly cooled ($\theta = -0.5$). The first test run was performed without an external magnetic field (Ht = 0) and the second with an external uniform magnetic field (Ht = 500) applied horizontally in the x-direction. Both runs were carried out for molten silicon (Table 1) with $Ra=10^6$ and Pr=0.054. A computational grid of 30x30x10 cells symmetrically clustered towards the walls was used for this purpose. In the case of no magnetic field the computed isotherms on the horizontal $z^* = 0.5$ mid-plane (Fig. 2a) and on the vertical $y^* = 0.5$ mid-plane (Fig. 2b) compare well with the computational results (Fig. 2c-d) of Ozoe and Okada [7]. In the case with the magnetic field applied, the computed isotherms (Fig. 3a-b) compare reasonably well (Fig. 3c-d) with those of Ozoe and Okada. This case is indicative of suppression of flow circulation by the strong externally applied magnetic field and the dominance of conduction in the process of heat transfer. The magnetic field in the x-direction thickens the thermal boundary layer in the vertical plane as is visible from the isotherms in the $y^* = 0.5$ vertical mid-sectional plane (Fig. 2b).

Closed container with solidification: In this case the cubical closed container was filled with molten steel having its top wall uniformly cooled below freezing temperature ($\theta = -1$) and the bottom wall uniformly heated ($\theta = 1$). The container was discretized with 20x20x20 grid cells that were clustered symmetrically towards all the walls. Two cases were run without the influence of the magnetic field (Ht = 0). One of the cases was in microgravity (g = 0.01 go) and the other with the full influence of gravity. The computed isotherms in the $y^* = 0.5$ vertical mid-plane (Fig. 4a-b) for the two cases indicate significant solidification occuring at the upper wall [20]. Evidently, in the microgravity case conduction is the dominant mode of heat transfer, whereas in the full gravity case heat transfer is carried out by both conduction and convection. The computed isotherms (Fig. 5a) and the contours of constant z-velocity components (Fig. 5b) on the horizontal $z^* = 0.5$ mid-plane in the full gravity case indicate strong centrally located downward jet and upward motion close to the walls thus forming a deformed thoroidal melt motion.

The solidification was then tested for the case where one vertical wall ($x^* = 0$) was kept uniformly hot ($\theta = 2$) and the opposite vertical wall ($x^* = 1$) was at a uniformly below freezing temperature ($\theta = -1$). In this case silicon was replaced by molten steel (Table 2). Two runs were performed with full gravity (g = go); one case without the magnetic field (Ht = 0) and the other with a strong external magnetic field (Ht=50) uniformly applied in the y-direction. A comparison of the computed isotherms (Fig. 6a-b) and velocity vector fields (Fig. 7a-b) in the $y^* = 0.5$ vertical mid-plane show a noticeable difference in the shape of the solid/melt interface when the magnetic field is applied. In this situation the thermally induced vorticity vector points mainly in the negative y-direction, while the magnetic field points in the positive y-direction thus strongly supressing the melt circulation and causing an increase in the amount of solid accrued on the vertical cold wall ($x^* = 0$).

In addition, two runs were performed in microgravity (g = 0.01 go); one case without the magnetic field (Ht = 0) and the other with a strong external magnetic field (Ht=50) uniformly applied in the y-direction. A comparison of the computed isotherms (Fig. 8a-b) in the $y^* = 0.5$ vertical mid-plane indicates a negligible difference in the shape of the solid/melt interface and the amount of the accrued solid.

Straight duct with solidification: The second configuration studied was a straight three-dimensional duct with a uniform melt temperature ($\theta = 2$) imposed at the duct inlet ($x^* = 0$). Along all four walls a cooling was specified as $\theta = 2 - 3.6 \sin(x^*\pi)$. Characteristic boundary conditions were used at the inlet, while specifying nothing at the exit. Instead, a non-reflecting boundary condition was enforced at the exit. The fluid used in this problem was molten steel (Table 2), which is characterised by the fact that it does not undergo a phase change isothermally, thereby giving rise to a sizable mushy region. The flow field was discretized with 50x20x20 grid cells that were clustered symmetrically towards the duct walls. Four computer runs were performed for this configuration.

The first test case represents a solidifying flow field in a microgravity environment (g = 0.01 go) without any magnetic field (Ht = 0). Computed solidified zones are clearly evident on all four walls of the duct from the computed velocity vector fields (Fig. 9a) in the horizontal ($z^* = 0.5$) mid-plane and the isotherms (Fig. 9b) in the vertical ($y^* = 0.5$) mid-plane. For all practical purposes the solution is doubly symmetric with respect to the longitudinal mid-planes.

Two additional test cases were then run in a

microgravity environment (g = 0.01 go) with uniform magnetic fields of Ht=10 and Ht=30, respectively, acting vertically downward. The influence of the magnetic fields is evident from the velocity vector plots (Figs. 10a-b) in the horizontal ($z^* = 0.5$) mid-plane depicting flattened velocity profiles. Consequently this leads to the thickening of thermal boundary layers at the vertical walls (Fig. 11a-b) and a slight decrease in the amount of solid phase accrued on the horizontal walls (Fig. 12a-b).

A fourth case was run with a full gravitational field (g = go) but without any magnetic field (Ht = 0). In this case strong asymmetry was noticed in the vertical ($y^* = 0.5$) mid-plane velocity pattern (Fig. 13a) and computed isotherms (Fig. 13b) due to thermal buoyancy resulting in a significantly more solid phase accrued on the bottom wall and less on the top wall as compared to the side walls. This is also evident from the computed isotherms in the vertical cross section plane ($x^* = 0.5$) of the duct (Fig. 14a). The computed non-uniform pressure at the exit plane (Fig. 14b) clearly demonstrates the benefits of using non-reflecting boundary conditions rather than forcing characteristic boundary conditions at the exit.

Figure 15 summarizes the effects of the magnetic field at full gravity and in microgravity for the closed container with solidification from a side wall. It is clear that the effect of the magnetic field is more pronounced (in this case it increases the amount of accrued solid) with the increase in gravity magnitude.

Conclusions

A complete analytical and numerical formulation has been developed for the theoretical prediction of phase change processes inside three-dimensional containers and passages with and without the influence of an externally applied steady magnetic field and arbitrary gravity vector. Computational results confirm that the magnetic field has a profound influence on the solidifying flow field since it weakens flow recirculation regions and causes distorted velocity profiles having overshoots close to the solid boundaries. Consequently, the temperature field also changes under the influence of the external magnetic field. This change influences convective heat transfer through the boundaries and reduces the amount of the solid phase accrued on undercooled walls. This is the result of higher melt velocity that is generated by the ponderomotive force close to the solid/liquid interface and, to a much lesser extent, by Joule heating. This demonstrates a possibility for the development of an active control algorithm for realistic three-dimensional solidification or melting since the magnetic fields can either increase or decrease the amount of acrued solid phase.

Acknowledgements

Authors are grateful for the useful references and comments provided by Prof. Vaughan R. Voller and Prof. Gita Talmage and for proofreading performed by Mr. Thomas J. Martin. All computations were performed remotely on the Cray-YMP computer at NASA Ames Research Center NAS facility and at Cray Research, Inc. in Eagan, Minnesota and post processed at Penn State on equipment donated by Apple Computer, Inc.

References

1. Chandrasekhar, S., Hydrodynamic and Hydromagnetic Stability, Dover Publication Inc., New York , 1961.

2. Stuetzer, O.M., "Magnetohydrodynamics and Electrohydrodynamics," *The Physics of Fluids,* vol. 5, No. 5 , 1962, pp. 534-544.

3. Ozoe, H. and Okada, K., "The Effect of the Direction of the External Magnetic Field on the Three-Dimensional Natural Convection in a Cubical Enclosure," *International Journal of Heat and Mass Transfer,* vol. 32, No. 2, 1989, pp. 1939-1954.

4. Vives, C., "Effects of a Magnetically Forced Convection During the Crystallization in Mould of Aluminum Alloys," *Journal of Crystal Growth,* vol. 94, 1989, pp. 739-750.

5. Motakef, S., "Magnetic Field Elimination of Convective Interference With Segregation During Vertical-Bridgman Growth of Doped Semiconductors", *Journal of Crystal Growth,* vol. 104, 1990, pp. 833-850.

6. Salcudean, M., and Sabhapathy, P., "Numerical Study of Liquid Encapsulated Czochralski Growth of Gallium Arsenide with and without an Axial Magnetic Field," ASME MD-Vol. 20, Computer Modeling and Simulation of Manufacturing Processes, Editors: Singh, B., Im, Y. T., Haque, I. and Altan, C., Book No. G00552, 1990, pp. 115-127.

7. Lee, S. and Dulikravich, G.S. "Magnetohydrodynamic Steady Flow Computations in Three Dimensions," *International Journal for Numerical Methods in Fluids,* vol. 13, No. 8, Oct. 1991, pp. 917-936.

8. Dulikravich, G. S., Kosovic, B. and Lee, S., "Solidification in Reduced Gravity With Magnetic Fields and Temperature-Dependent Physical Properties", HTD-Vol. 175/MD-Vol.25, pp. 61-73, Heat and Mass Transfer in Solidification Processing, Editors: S.G. Advani and C. Beckermann, ASME WAM'91, Atlanta, GA, Dec. 1-6, 1991, pp.61-73.

9. Dulikravich, G.S. and Kosovic, B., "Solidification of Variable Property Melts Under the Influence of Low Gravity, Magnetic Fields and Electric Fields," AIAA paper 92-0694, AIAA Aerospace Sciences Meeting, Reno, NV, Jan. 6-9,1992.

10. Kosovic, B., Dulikravich, G.S. and Lee, S., "Freezing Under the Influence of a Magnetic Field: Computer Simulation", Proc. of ICHMT Internat. Symp. on Macroscopic and Microscopic Heat & Mass Transfer in Biomed. Eng., Editors: K.Diller and A. Shitzer, Athens, Greece, Sept. 2-6, 1991, Elsevier Press, pp. 307-326.

11. Dulikravich, G. S., Kosovic, B., and Lee, S., "Magnetized Fiber Orientation Control in Solidifying Composites: Numerical Simulation", 28th ASME National Heat Transfer Conference, San Diego, CA., August 9-12, 1992, Proceedings of the Symposium on Transport Phenomena in Materials Processing and Manufacturing, Editors: M. Charmchi et al., HTD-Vol. 196, pp. 135-144; also to appear in *Journal of Heat Transfer,* Spring 1993.

12. Gray, D.D. and Giorgini, A., "The Validity of the Boussinesq Approximation for Liquids and Gases," *International Journal of Heat and Mass Transfer*, vol. 19, 1976, pp. 545-551.

13. Voller, V.R. and Swaminathan, C.R., "General Source-Based Method for Solidification Phase Change", *Numerical Heat Transfer, Part B*, vol. 19, 1991, pp. 175-189.

14. Poirier, D. and Salcudean, M., "On Numerical Methods Used in Mathematical Modeling of Phase Change in Liquid Metals", ASME paper 86-WAM/HT-22, Anaheim, CA, Dec. 7-12, 1986.

15. Chorin, J.A., "A Numerical Method for Solving Incompressible Viscous Flow Problems," *Journal of Computational Physics*, vol. 2, 1967, pp. 12-26.

16. Lee, S. and Dulikravich, G.S., "Performance Analysis of DMR Method for Acceleration of Iterative Algorithms," AIAA paper 91-0241, AIAA Aerospace Sciences Meeting, Reno, NV, January 7-10, 1991.

17. Jameson, A., Schmidt, W. and Turkel, E., "Numerical Solution of the Euler Equations by Finite Volume Methods Using Runge-Kutta Time-Stepping Scheme," AIAA paper 81-1259, AIAA Computational Fluid Dynamics Conference, Palo Alto, CA, June 1981.

18. Thomson, K. W., "Time-dependent Boundary Conditions for Hyperbolic Systems, I," *Journal of Computational Physics*, vol. 68, 1987, pp. 1-24.

19. Thomson, K. W., "Time-dependent Boundary Conditions for Hyperbolic Systems, II," *Journal of Computational Physics*, vol. 89, 1990, pp. 439-461.

20. Kerr, R. C., Woods, A. W., Worster, M. G., and Huppert, H. E., " Solidification of an Alloy Cooled From Above. Part 1. Equilibrium Growth," *Journal of Fluid Mechanics*, vol. 216, 1990, pp. 323-342.

	Steel melt	Silicon melt
Re	100	200
Pr	0.4167	0.054
Gr	1000	1.85×10^6
Ec	5.56×10^{-10}	7.87×10^{-8}
Ht	0, 10, 30	0, 500
Pm	0.01	0.01

Table 1. Nondimensional input parameters.

C_{pl} [J kg^{-1} K^{-1}]	788
C_{ps} [J kg^{-1} K^{-1}]	465.4 + 0.1336 T
k_l [W m^{-1} K^{-1}]	12.29
k_s [W m^{-1} K^{-1}]	8.16
T_l [K]	1727
T_s [K]	1670
L [J kg^{-1}]	265200

Table 2. Physical properties for molten steel

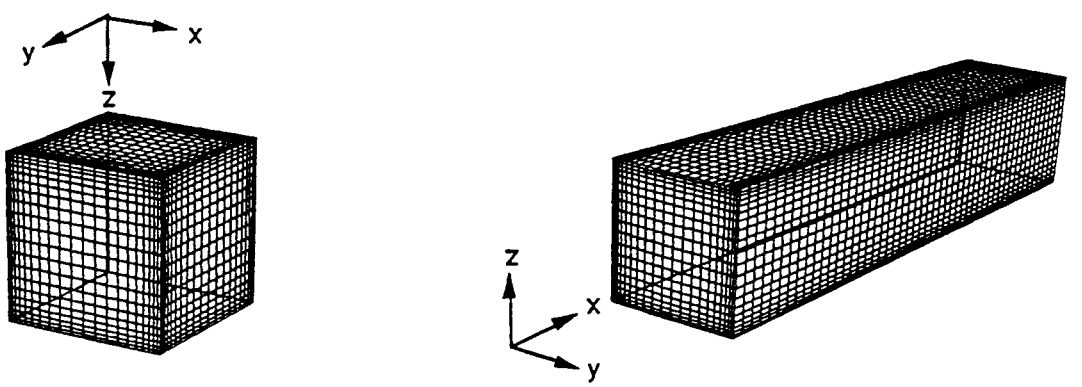

Fig. 1 Test configurations and computational grids;
a) closed container, b) straight duct

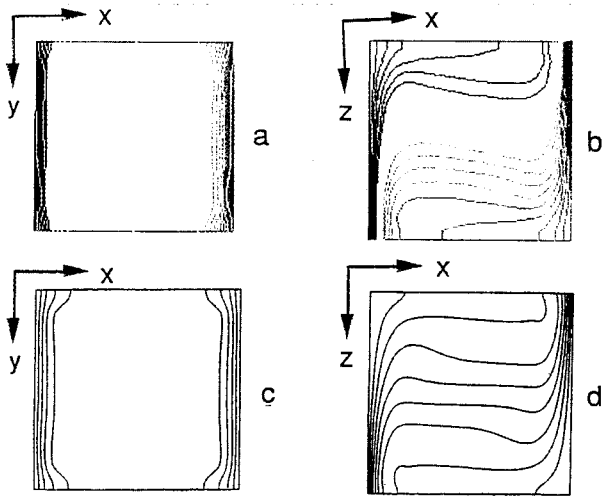

Fig. 2 Isotherms for closed container without solidification (Ht = 0): a) $z^* = 0.5$ computed; b) $y^* = 0.5$ computed; c) $z^* = 0.5$ from [3]; d) $y^* = 0.5$ from [3].

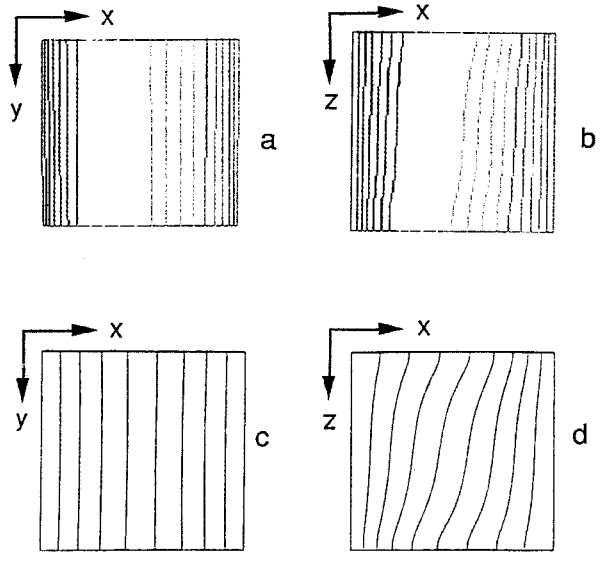

Fig. 3 Isotherms for closed container without solidification (Ht = 500): a) $z^* = 0.5$ computed; b) $y^* = 0.5$ computed; c) $z^* = 0.5$ from [3]; d) $y^* = 0.5$ from [3].

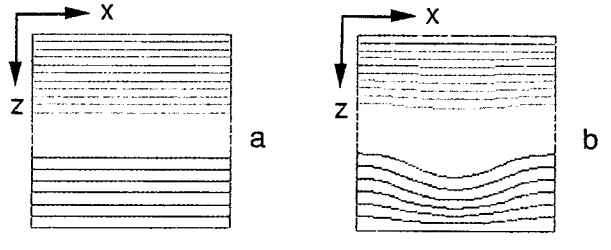

Fig. 4 Isotherms for closed container with solidification ($y^* = 0.5$, Ht = 0): a) g = 0.01go; b) g = go.

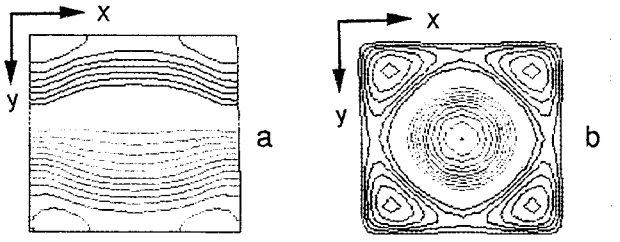

Fig. 5 Closed container with solidification ($z^* = 0.5$, g = go, Ht = 0): a) isotherms; b) constant z-velocity contours.

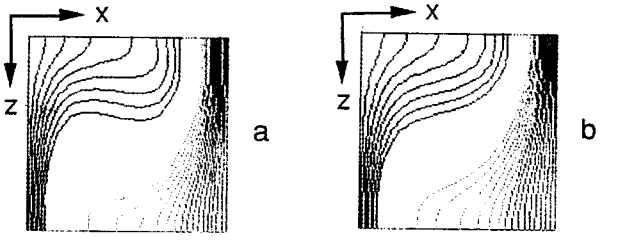

Fig. 6 Isotherms for closed container with solidification ($y^* = 0.5$, g = go): a) Ht = 0; b) Ht = 50.

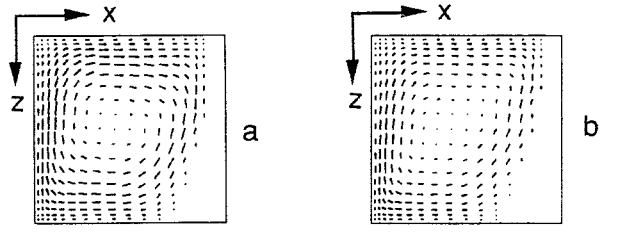

Fig. 7 Velocity fields for closed container with solidification ($y^* = 0.5$, g = go): a) Ht = 0; b) Ht = 50.

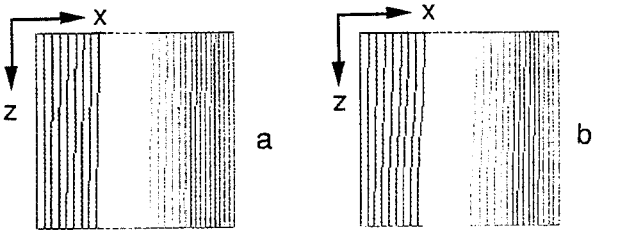

Fig. 8 Isotherms for closed container with solidification ($y^* = 0.5$, g = 0.01go): a) Ht = 0; b) Ht = 50.

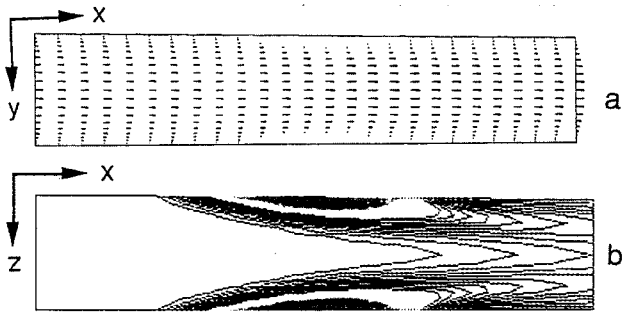

Fig. 9 Straight duct with solidification ($g = 0.01g_o$, $Ht = 0$): a) velocity field at $z^* = 0.5$; b) isotherms at $y^* = 0.5$.

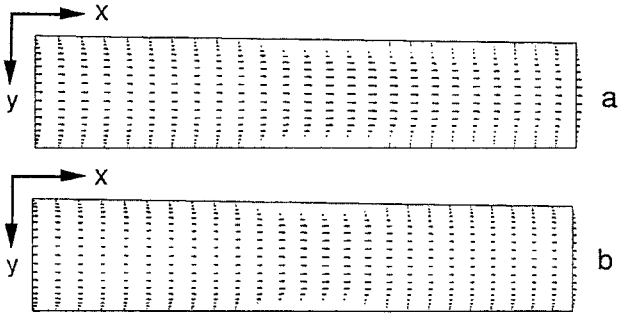

Fig. 10 Velocity fields in straight duct with solidification ($z^* = 0.5$, $g = 0.01g_o$): a) $Ht = 10$; b) $Ht = 30$.

Fig. 11 Isotherms in straight duct with solidification ($y^* = 0.5$, $g = 0.01g_o$): a) $Ht = 10$; b) $Ht = 30$.

Fig. 12 Isotherms in straight duct with solidification ($z^* = 0.5$, $g = 0.01g_o$): a) $Ht = 10$; b) $Ht = 30$.

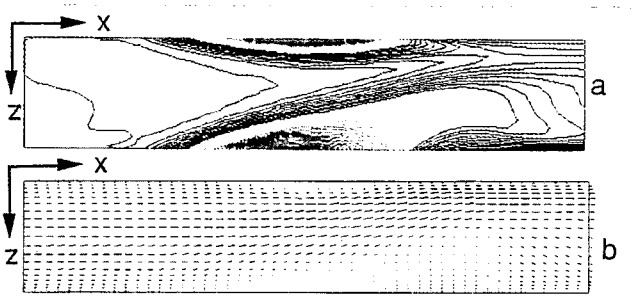

Fig. 13 Straight duct with solidification ($y^* = 0.5$, $g = g_o$, $Ht = 0$): a) velocity field; b) isotherms.

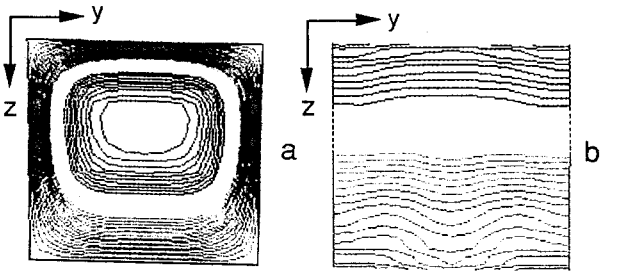

Fig. 14 Straight duct with solidification ($g = g_o$, $Ht = 0$): a) velocity field at $x^* = 0.5$; b) pressure at the exit $x^* = 1$.

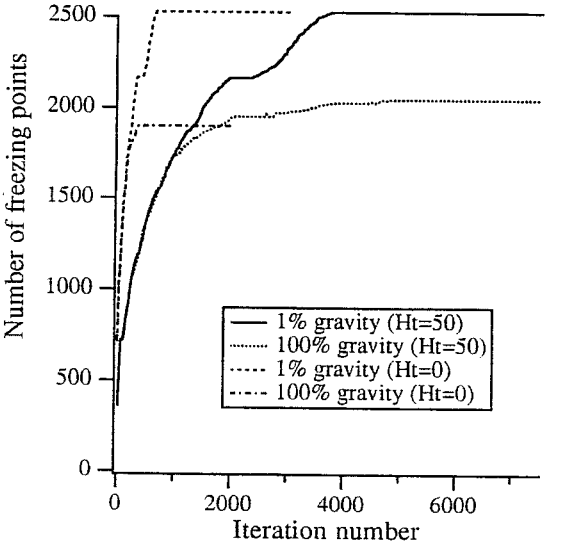

Fig. 15 Convergence histories for solidification in a closed container filled with molten steel (side freezing).